ACS APPLIED MATERIALS & INTERFACES

Research Article

www.acsami.org

Characterization of Biodegradable Polyurethane Nanoparticles and Thermally Induced Self-Assembly in Water Dispersion

Chun-Wei Ou,[†] Chiu-Hun Su,[‡] U-Ser Jeng,[§] and Shan-hui Hsu[†,*]

[†]Institute of Polymer Science and Engineering, National Taiwan University, Taipei, Taiwan

[‡]Material and Chemical Research Laboratories, Industrial Technology Research Institute, Hsinchu, Taiwan

[§]National Synchrotron Radiation Research Center, Hsinchu, Taiwan

Supporting Information

ABSTRACT: Waterborne polyurethanes (PU) with different compositions of biodegradable oligodiols as the soft segment were synthesized as nanoparticles (NPs) in this study. Using dynamic light scattering (DLS), multiangle light scattering (MALS), transmission electron microscopy (TEM), and small-angle X-ray scattering (SAXS), we demonstrated that these NPs were compact spheres with different shape factors. The temperature-dependent swelling of the PU NPs in water was distinct. In particular, PU NPs with 80 mol % polycaprolactone (PCL) diol and 20 mol % poly(L-lactide) (PLLA) diol as the soft segment had significant swelling (~450%) at 37 °C. This was accompanied by a sol−gel transition observed in about 2 min for the NP dispersion. The thermally induced swelling and self-assembly of these NPs were associated with the secondary force (mainly hydrogen bonding) and degree of crystallinity, which depended on the soft segment compositions. The thermo-responsiveness of the PU NPs with mixed biodegradable oligodiols may be employed to design smart biodegradable carriers for delivery of cells or drugs near body temperature.

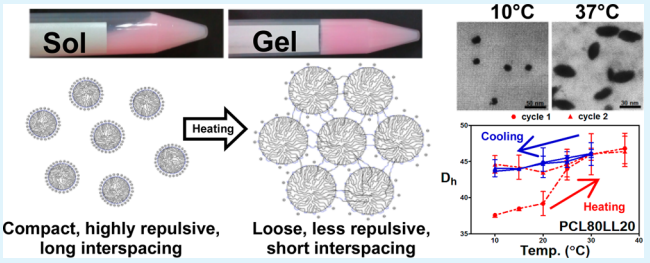

KEYWORDS: *waterborne polyurethane, asymmetrical flow field-flow fractionation (AFFFF), small-angle X-ray scattering (SAXS), biodegradable*

1. INTRODUCTION

Hydrogels are composed of hydrophilic polymer chains in three-dimensional structure. The excellent water-retaining properties have made them an important category of biomedical materials for more than fifty years. The existing commercial products of hydrogels include contact lens, wound dressings, drug carriers, and so on. Hydrogels are also regarded as good cell carriers in applications such as tissue engineering.[1,2] Stimuli-responsive hydrogels can undergo phase transitions in response to changes of environmental conditions such as temperature, pH value, and ionic strength. By varying the temperature, the secondary interactions between temperature-responsive polymer chains are affected, leading to a significant change in volume.[3] On the other hand, pH-responsive polymers contain ionic segment in backbone that is sensitive to pH value and ionic strength. Because of the unique properties, the pH-responsive materials are widely studied as delivery systems in response to pH changes in different parts of human body.[4−6] The lack of biodegradability and poor mechanical properties after swelling have yet limited the applications of stimuli-responsive hydrogels in the biomedical field.

Polyurethane (PU) with excellent mechanical properties and biocompatibility has been widely used in medical devices.[7−9] The synthesis of PU by waterborne procedures may substantially reduce the cost in after-treatment and the amount of organic solvent that can cause environmental pollution.[10] The chemicals used to synthesize waterborne PU mainly include diisocyanates, oligodiols, and chain extenders. An internal or external emulsifier is needed during the synthesis of waterborne PU, which stabilizes the dispersion. The emulsifier can also increase the sensitivity of PU particles to the environmental stimulus.[11]

Hydrogels of PU backbone can provide good biocompatibility and avoid the loss of mechanical strength that occurs in a traditional absorbent polymer after swelling.[12−14] Traditional waterborne PU is nonbiodegradable. By introducing biodegradable components such as an ester-based oligodiol in the soft segment, the biodegradability can be conveniently modulated.[15,16] The chemical structure of PU hydrogels is both important for the sol−gel transition[17] and the biodegradability.[18]

Here in this study, we investigated the effect of different soft segments on the dispersion and phase transition of biodegradable PU nanoparticles (NPs) in water. First, novel biodegradable PU NPs were synthesized from a waterborne

Received: January 11, 2014
Accepted: March 19, 2014
Published: April 1, 2014

procedure. The chemical structure employed a mixture of ester-based oligodiols, i.e., one was polycaprolactone diol (PCL diol), and the other was polyethylene butylene adipate diol (PEBA diol) or poly(L-lactide) diol (PLLA diol). By adjusting the molecular ratio of the two oligodiols, different PU NPs were synthesized. The size of PU NPs in water was investigated by various analytical techniques. The temperature-dependent changes in size and zeta potential, the swelling ratio, and the rheological properties were also examined. We demonstrated that by fine-tuning the chemical structure and molar ratio of the oligodiols, we were able to modulate the physicochemical properties and smartness of these green NPs for potential biomedical applications.

2. MATERIALS AND METHODS

2.1. Synthesis of Waterborne Biodegradable PU. PU in this study was synthesized from an optimized waterborne procedure. Three types of oligodiols with similar molecular weight (M_n) ~2000 were used as the soft segment, which included polycaprolactone diol (PCL diol, Sigma-Aldrich), polyethylene butylene adipate diol (PEBA diol, Greco), and PLLA diol. The PLLA diol was synthesized from the ring-opening polymerization of L-lactide (Purac) by 1,3-propanediol (Alfa Aesar, UK) with 0.03% stannous octoate ($Sn(Oct)_2$, Alfa Aesar) as the catalyst. PCL diol in combination with another type of oligodiols in different molar ratios were first added to the vessel and stirred for 30 min. Prepolymerization was carried out at appropriate temperature by adding isophorone diisocyanate (IPDI, Evonik Degussa GmbH) with oligodiols under nitrogen atmosphere for 3 h in the presence of $Sn(Oct)_2$ as the catalyst. Afterward, 2,2-bis(hydroxymethyl) propionic acid (DMPA, Sigma) and 0.27% of methyl ethyl ketone (MEK, J.T. Baker) were added to the reactor under reflux. Triethylamine (TEA, R.D.H) was then added to neutralize the carboxylic groups in DMPA at 45 °C for 30 min. Finally, ethylenediamine (EDA, Tedia) diluted with deionized water was added to the reactor under vigorous stirring. The stoichiometric ratio of IPDI/oligodiols/DMPA/EDA/TEA was 3.52:1:1:1.52:1.[19] The residual solvent and neutralizing agent were then removed by vacuum distillation. These waterborne PU were designated as the molar ratio of total amount in soft segment. For example, PCL80LL20 represents the sample with 80 mol % PCL diol and 20 mol % PLLA diol in soft segment as shown in Table 1.

Table 1. Designation and Glass Transition Temperature (T_g) of Biodegradable Waterborne PU NPs Prepared in This Study

	molar ratio (mol %) in the soft segment				
designation	PCL diol	PLLA diol	PEBA diol	zeta potential (mV)	T_g (°C)
PCL100	100	0	0	−57.63 ± 0.95	−52
PCL80LL20	80	20	0	−54.81 ± 1.03	−54.5
PCL60LL40	60	40	0	−57.63 ± 0.96	−46.6
PCL80EB20	80	0	20	−59.06 ± 0.63	−47.3

[a] T_g for PLLA diol was ~25 °C, and was much lower (below zero) for PCL diol and PEBA diol. The melting point of PCL diol was ~50 °C and that of PEBA was ~25 °C.

2.2. Asymmetric Flow Field-Flow Fractionation (AFFFF) Analysis. The PU NP was characterized at 25 °C using AFFFF (Eclipse 4, Wyatt, USA) at 1 mL min^{-1}. To avoid channel blocking, we used 0.1 M $NaNO_3$ buffer as the eluent. Dynamic light scattering (DLS; Wyatt's DynaPro NanoStar), multiangle laser light scattering (MALS; Dawn Heleos II, Wyatt), and differential refractometer (dn/dc) measurements (Optilab T-rEX, Wyatt) were equipped to determine the hydrodynamic radius (R_h), radius of gyration (R_g), and apparent molecular weight ($M_{w,\,NP}$) for each NP.

2.3. Differential Scanning Calorimeter (DSC). Dried PU NPs (4 mg) were placed in an aluminum sample pan and sealed for analysis by a differential scanning calorimeter (DSC; Perkin-Elmer Pyris 6, USA) with nitrogen purging. The temperature range was from −80 to 300 °C with a heating rate of 10 °C/min. T_g was defined as the maximum in the first derivative of heatflow (the heat capacity change at the transition).

2.4. Hydrodynamic Size and Zeta Potential of PU NPs. The PU dispersion was diluted with deionized water to a concentration of 3000 ppm for analysis of size and zeta potential. The hydrodynamic size (D_h) of PU NPs was measured by DLS using a cumulant method. The zeta potential was determined based on the electrophoretic light scattering measurements. Both measurements were carried out at varying temperature in the range from 10 to 37 °C of size and zeta potential by a submicrometer particle analyzer (Delsa Nano Analyzer, Beckman Coulter). The values presented were the arithmetic means (± standard deviation) from three different positions on the samples.

2.5. Small-Angle X-ray Light Scattering (SAXS). PU NPs were investigated by SAXS at the beamline 23A of National Synchrotron Radiation Research Center at Hsinchu, Taiwan. The photon energy was at about 10 keV. The ranges of scattering vector (Q) were from 0 to 0.1 ($angstrom^{-1}$) for SAXS. By ignoring the Q-values that were close to zero because of the beam stop, the SAXS profiles were obtained at varying temperature in a range from 20 to 37 °C. The radius of gyration (R_g) were estimated by the Guinier analysis under the condition of $qR_g < 1.3$. On the basis of the Kratky analysis, the product of the intensity and square of the scattering vector (q^2) was plotted against the scattering vector (q). The invariant Q could be obtained from the integral between $q = 0$ to $q = 0.2$ (A^{-1}). The volume (V) and molecular weight ($M_{w,\,NP}$) of PU NP could be determined by the following formulas, $V = 2\pi I(0)/Q$ and $M_{w,\,NP} = V\rho N_A$, where $I(0)$, ρ, and N_A represent the absolute intensity, density, and Avogadro's number, respectively.

2.6. Transmission Electron Microscopy (TEM). PU NPs were examined by TEM (JEM-1200EX II, JEOL, Japan) using 80 kV electron beam. The PU dispersion were first diluted to 500 ppm, cast on a copper grid, and dried at room temperature overnight. The samples were then stained by 2% phosphotungstic acid (Alfa Aesar) for 1 min before examination.

2.7. Rheological Measurements. Rheological properties were measured by a rheometer (RS-5, TA Instruments) with a cone and plate geometry. The angle of the cone was 2° and the diameter was 40 mm. An environmental control chamber was applied to prevent sample drying. PU dispersion of 0.7 mL was injected onto the plate and the temperature was adjusted to 37 °C by a Peltier system. Storage and loss shear modulus values were measured with a constant frequency 1 Hz and 1% strain against time.

2.8. Swelling Test. The PU dispersion was first gelled at 37 °C for 48 h. The shape and dimension of the gels were cylinders with 1.5 cm diameter and 1 cm height. Samples were immersed into 20 mL of deionized water at 37 °C for 24 h. The surface was removed of excess water and the samples were weighed (W_e). After that, the samples were lyophilized for 24 h by a freeze-dryer (FDU-1200, Eyela) and the dry weights were obtained (W_d). The swelling ratio of the gel was obtained by the following equation.

$$\text{swelling ratio}\ (\%) = (W_e - W_d)/W_d \times 100\%$$

2.9. X-ray Diffraction (XRD) Analysis. The crystalline from of films cast from PU NPs was investigated by XRD using a X-ray diffractometer (Bede D1, UK) in the scan range from $2\theta = 10$ to 30°.

2.10. Fourier Transform Infrared Spectroscopy (FT-IR) Analysis. The FT-IR spectra of films cast from PU NPs were obtained using a FT-IR spectrophotometer (Spectrum 100, Perkin-Elmer, USA). Each sample was scanned 16 times at a resolution of 1 cm^{-1} over the frequency range of 4000−600 cm^{-1}. Curve fitting was based on linear analysis to resolve the combination of Lorentzian and Gaussian curve shapes.

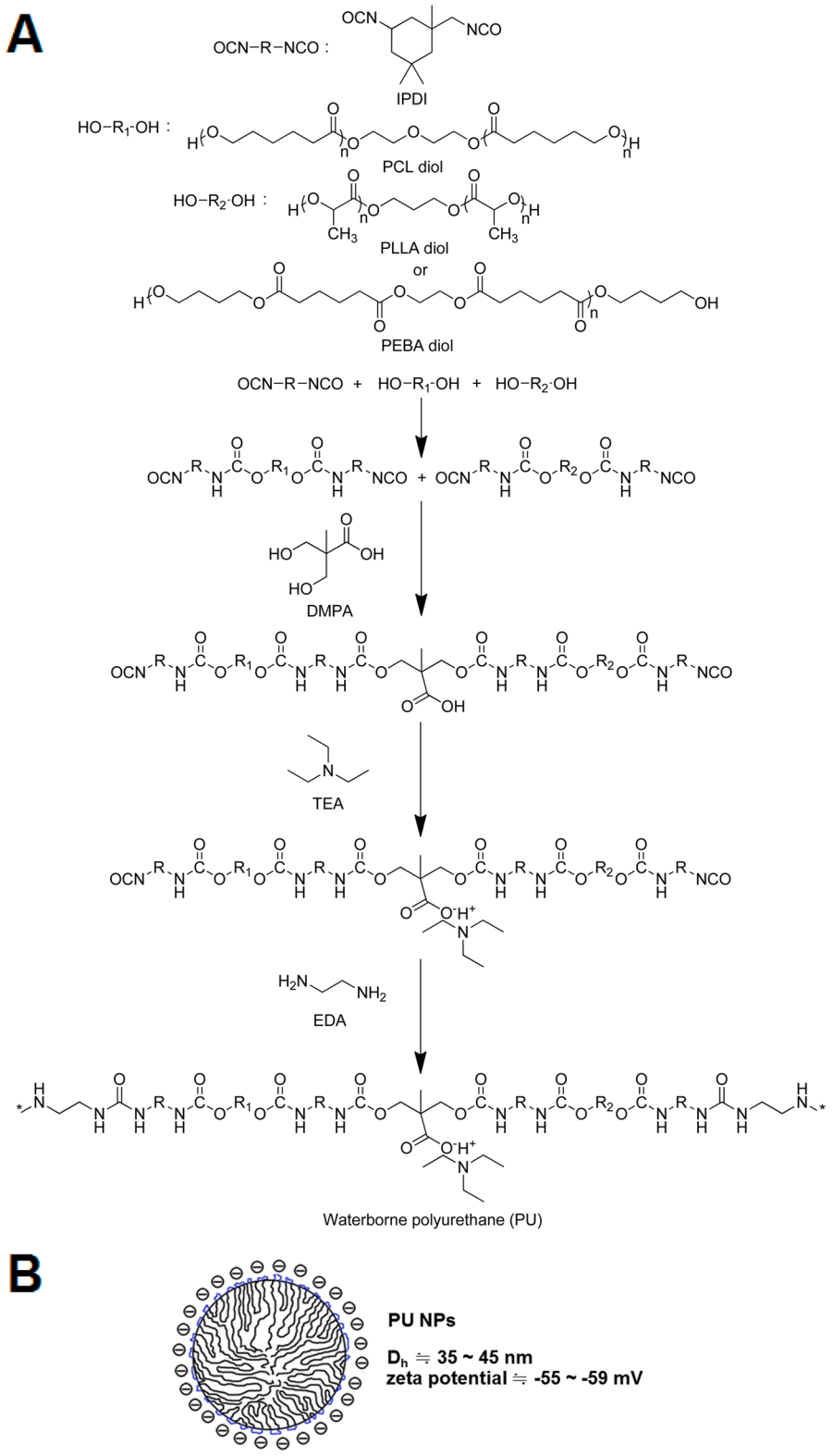

Figure 1. (A) Chemical structures of waterborne PU and (B) the sketch of PU NP synthesized in this study.

3. RESULTS

3.1. Synthesis and Basic Properties of Waterborne Biodegradable PU. *3.1.1. Synthesis of PU NP Dispersions.* PUs with different soft segment compositions were successfully synthesized by an aqueous procedure. Figure 1 shows the chemical structures for the three different polyester-based oligodiols and the four biodegradable PUs prepared in this study. The zeta potential for various PU NPs is also listed in Table 1. The zeta potential value fell into a range of −60 to −54 mV, indicating the stability of the NP dispersions.

3.1.2. AFFFF Analysis of PU NPs. PU NPs were fractionated according to size through the induced cross-flow of AFFFF-MALS-DLS analysis to obtain the information regarding the

dx.doi.org/10.1021/am500213t | ACS Appl. Mater. Interfaces 2014, 6, 5685−5694

Table 2. Characterization of PU NPs by AFFFF-MALS/DLS at 25°C

	single chain						
PU	M_w ($\times 10^2$ kDa)	PDI (M_w/M_n)	R_h (nm)	R_g (nm)	R_g/R_h (shape factor)	$M_{w,NP}$ ($\times 10^4$ kDa)	N_{agg}
PCL100	1.65	1.20	18.0 ± 0.3	22.5 ± 3.8	1.27	6.60 ± 0.16	400
PCL80LL20	1.87	1.93	13.5 ± 0.3	19.2 ± 2.9	1.42	3.19 ± 0.05	170
PCL60LL40	1.42	1.93	15.9 ± 0.3	26.4 ± 2.4	1.66	4.77 ± 0.08	336
PCL80EB20	1.87	1.30	14.9 ± 0.2	24.4 ± 2.9	1.64	5.22 ± 0.09	279

hydrodynamic radius (R_h), radius of gyration (R_g), and molecular weight of NPs ($M_{w,NP}$). The results of R_h, R_g, and $M_{w,NP}$ are summarized in Table 2. The R_g value (19.2 nm) of PCL80LL20 was the lowest among the four PU NPs. By contrast, the R_g value (26.4 nm) of PCL60LL40 was larger than that of PCL100. The shape factor (R_g/R_h) is also listed in Table 2. PCL100 NPs showed a shape factor of 1.27. When the soft segment contained a second oligodiol, the shape factor increased. The largest shape factor (1.66) was observed in PCL60LL40. By comparing the molecular weight of single PU chain from GPC and the apparent molecular weight of PU NPs ($M_{w,NP}$) from AFFFF-MALS, the number of aggregation (N_{agg}) could be estimated and is listed in Table 2. Among various NPs, PCL80LL20 had a lower N_{agg} (~170) than PCL100 and PCL60LL40 (N_{agg} ~400).

3.1.3. DSC Analysis for T_g of PU NPs. The glass transition temperature (T_g) of different PUs and oligodiols measured by DSC is listed in Table 1. Results showed that PCL100 had a T_g at −52 °C. PCL80LL20 had a lower T_g than PCL100, while PCL60LL40 had a higher T_g than PCL100 and PCL80LL20. The difference in T_g values among the four PUs, however, was smaller than 8 °C.

3.2. Thermal Dependence of the NP Properties. *3.2.1. Hydrodynamic Size and Zeta Potential by DLS.* The thermal dependence of D_h for the PU NPs from 10 to 37 °C is displayed in Figure 2. Experiments were carried out in two temperature cycles including twice heating and cooling processes. PCL100 NPs could maintain D_h in the range between 37.6 to 38 nm. No size change was observed for PCL100 NPs in any cycle. On the other hand, the size of PCL80LL20 NPs increased in the first heating cycle. The size increase was about 10 nm and was not reversible. No significant change was observed for PCL80LL20 in the second thermal cycle. PCL60LL40 and PCL80EB20 NPs showed similar changes as PCL80LL20. The size increases from 10 to 37 °C were about 10 and 6 nm for PCL60LL40 and PCL80EB20 each, which were much lower than that for PCL80LL20. In particular, the irreversible size changes for these PU NPs occurred at temperature above 25 °C, i.e., the size changes between 10 to 25 °C were reversible. Overall, the thermal responsiveness of PU NPs was in the order of PCL80LL20 > PCL60LL40 > PCL80EB20 > PCL100. The effects of varying temperature on zeta potential are shown in the Supporting Information (Figure S1). The zeta potential was retained in the range of −55 to −59 mV for PCL100 NPs, while that of PCL80LL20 NPs increased with the increasing temperature, to about −40 mV (less negative). The same trend of zeta potential (i.e., charge density decrease) was found in both PCL60LL40 and PCL80EB20 NPs.

3.2.2. Size of PU NPs by TEM. TEM images for PU NPs are displayed in Figure 3. The NPs of PCL100 were nearly spherical in shape with a diameter of 35 nm at 10 °C. PCL80LL20 NPs were also in spherical shape with a size ~30 nm at 10 °C, but they transformed into rodlike particles with a

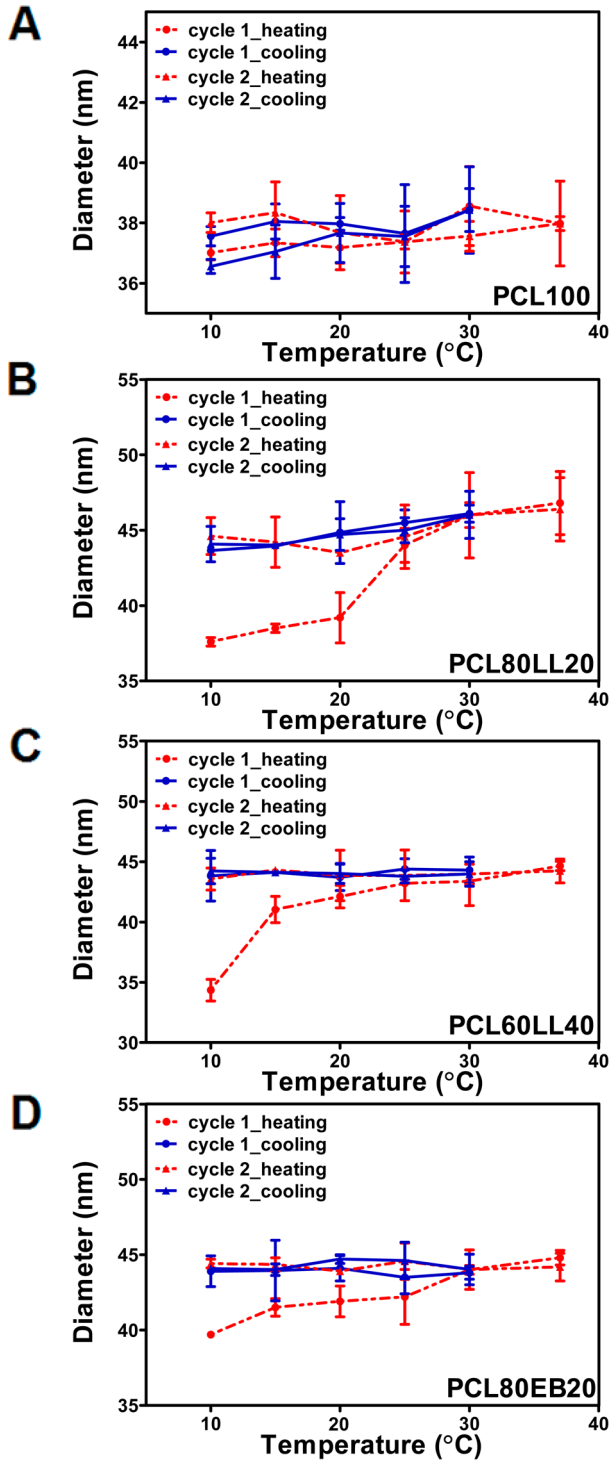

Figure 2. Thermal reversibility of the size for various PU NPs: (A) PCL100, (B) PCL80LL20, (C) PCL60LL40, and (D) PCL80EB20.

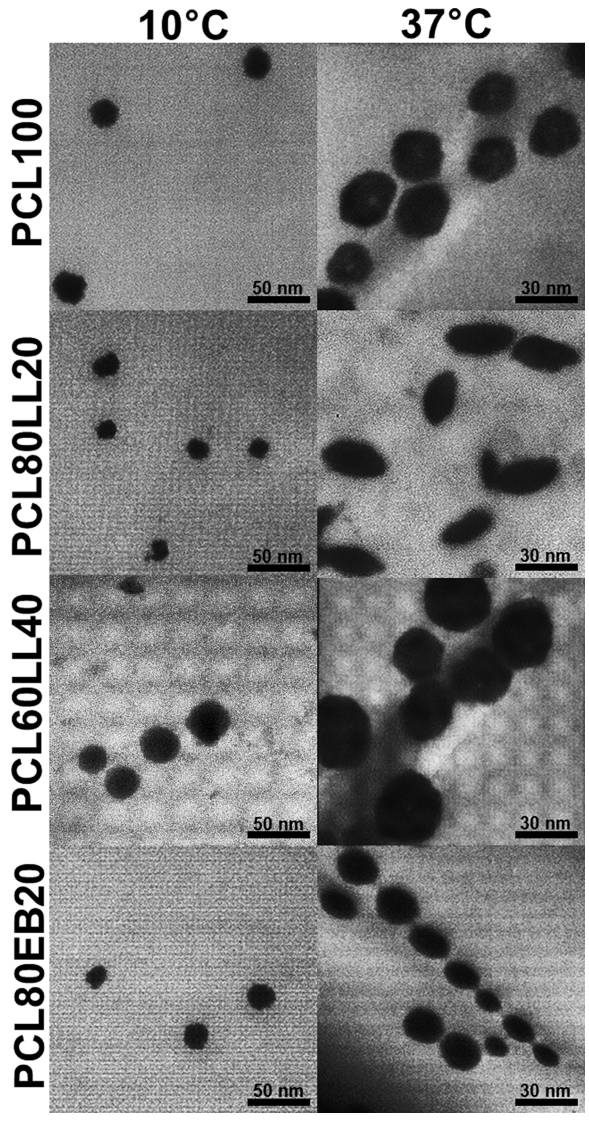

Figure 3. TEM images for various PU NPs at two different temperatures, 10 and 37 °C.

larger size at 37 °C. PCL60LL40 NPs also showed a larger size at 37 °C, yet the shape was more spherical than PCL80LL20 NPs at the same temperature. PCL80EB20 NPs demonstrated a similar trend of size change as PCL60LL40 NPs upon temperature increase, i.e., they became larger at 37 °C and kept relatively spherical in shape.

3.2.3. SAXS Profiles for PU NP Dispersions. The results of SAXS for PU NP dispersions are displayed in Figure 4. As the PCL content in the soft segment increased, the SAXS curve shifted the characteristic peak to the right (high q-range). The corresponding d-spacing of this characteristic peak was about 20 nm. The values of R_g obtained from the Guinier analysis under low-q range are shown in Table 3. The shape factor based on the R_g value (SAXS) and R_h (= $D_h/2$, from DLS) is also listed. The shape factors for all PU NPs were closed to 1 at low temperatures. Among the four polymers, PCL80LL20 NPs at 37 °C showed a particularly large shape factor at 1.33, i.e., more rodlike morphology at 37 °C. Simultaneously, $M_{w,\,NP}$ could be estimated from SAXS data by the Kratky analysis and the results are shown in Table 4. Based on the estimation, PCL80EB20 NPs had the highest molecular weight of ~5.4 × 10^4 kDa and PCL60LL40 NPs had the lowest molecular weight of ~3.4 × 10^4 kDa. The values of N_{agg} obtained from such a method were close among the four PU NPs (~270). The volumetric changes between 10 and 37 °C calculated based on the change of sizes from DLS are also listed in Table 4. The largest change in volume (~210%) was predicted for PCL80LL20 NPs. Only a small volume change (~110%) was estimated for PCL100 NPs.

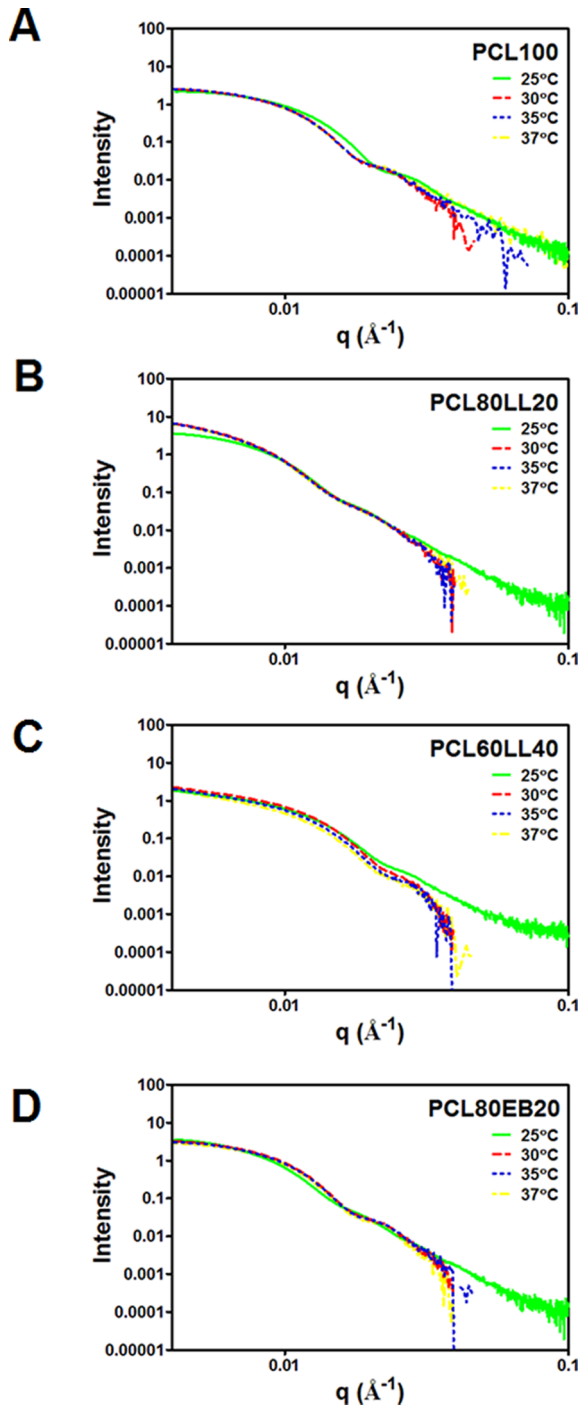

Figure 4. SAXS profiles for (A) PCL100, (B) PCL80LL20, (C) PCL60LL40, and (D) PCL80EB20.

3.3. Thermally Induced Self-Assembly and Behavior Change. *3.3.1. Rheological and Swelling Behavior of PU NP Dispersions at 37 °C.* The swelling ratio of the PU NPs at 37

dx.doi.org/10.1021/am500213t | ACS Appl. Mater. Interfaces 2014, 6, 5685−5694

Table 3. Hydrodynamic Radius (R_h) and Radius of Gyration (R_g) Measured by DLS and SAXS

	R_h (nm)			R_g (nm)		R_g/R_h (shape factor)		volumetric change (%)	
PU NPs	10 °C	25 °C	37 °C	25 °C	37 °C	25 °C	37 °C	37 °C/25 °C	37 °C/10 °C
PCL100	18.5 ± 0.2	18.7 ± 0.5	19.3 ± 0.7	19.0 ± 0.6	21.2 ± 0.4	1.02	1.10	109	112
PCL80LL20	18.3 ± 0.3	22.0 ± 0.5	23.4 ± 0.8	18.8 ± 0.2	31.1 ± 0.2	0.85	1.33	120	209
PCL60LL40	17.2 ± 0.9	21.6 ± 0.1	22.1 ± 0.2	17.8 ± 0.5	23.1 ± 0.4	0.82	1.10	107	183
PCL80EB20	19.9 ± 0.2	21.1 ± 0.9	22.3 ± 1.0	21.4 ± 0.3	22.3 ± 0.1	1.01	1.00	118	142

Table 4. Molecular Weight of PU and Apparent Molecular Weight of Each NP ($M_{w,\ NP}$) from SAXS at 25°C

PU NPs	$M_{w,\ NP}$ (× 10^4 kDa)	N_{agg}
PCL100	4.33	262
PCL80LL20	4.91	262
PCL60LL40	3.88	273
PCL80EB20	5.58	298

°C is shown in Figure 5A. The swelling ratio of PCL100 was close to 0. Each of the other three PU NPs had swelling ratios greater than 300%. The highest swelling ratio (~450%) was observed for PCL80LL20. The temperature-induced swelling phenomenon was consistent with the size and volumetric changes (Table 3). A summary of size alteration for different PU NPs is presented in Figure 5B. PCL100 NPs had no thermal responsiveness, whereas the other three PU NPs showed an increase of size and zeta potential upon heating.

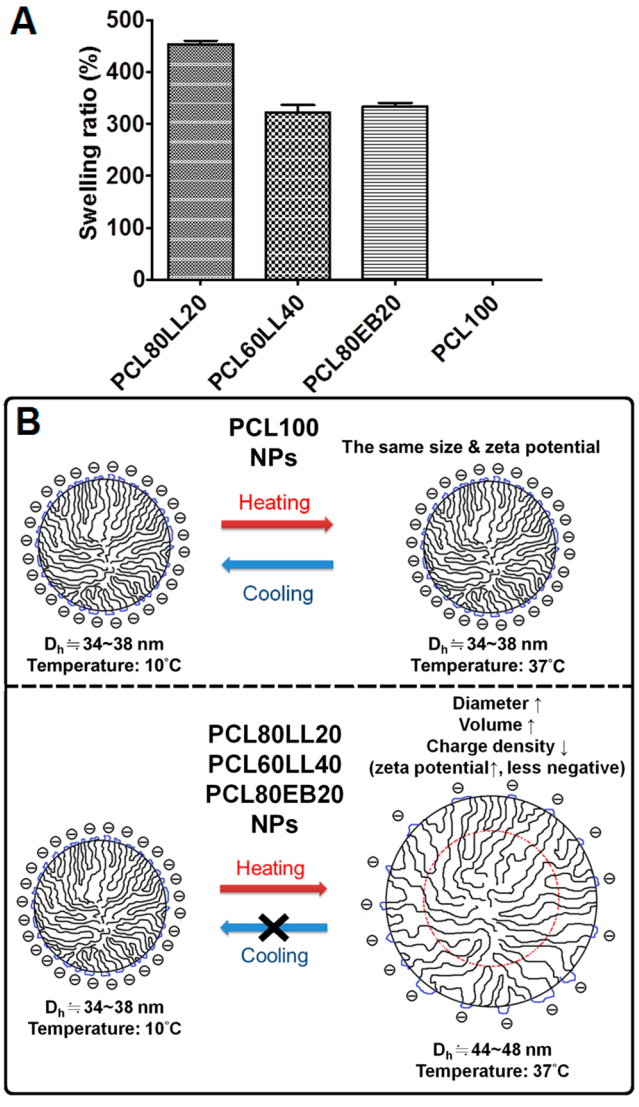

Figure 5. (A) Equilibrium swelling ratio (%) of waterborne biodegradable PU NP dispersions at 37 °C. (B) A summary of swelling and the size change for the PU NPs.

The rheological properties expressed as the shear storage modulus (G') and loss modulus (G'') of the PU NP dispersion upon a temperature rise to 37 °C are shown in Figure 6. PCL100 had no considerable phase transition between 10 and 37 °C. On the other hand, a sol−gel transition was observed for PCL80LL20, PCL60LL40, and PCL80EB20 NP dispersion when placed at 37 °C. The PCL80LL20 NP dispersion demonstrated the fastest gelation (~127 s). PCL60LL40 and PCL80EB20 each showed phase transition at 742 and 1103 s. A greater G' value was observed for PCL80LL20 during gelation. The equilibrium gel modulus is listed in Table 5. PCL80LL20 had the highest gel modulus (>1 kPa) followed by PCL60LL40.

3.3.2. Characterization of Dried PU NPs by XRD and SAXS. XRD profiles of the polymers are shown in Figure 7. PCL100 revealed a broad amorphous curve and no evident crystalline peak. On the other hand, PCL80LL20 showed crystalline peaks of PLLA (at $2\theta = 16.5°$) as well as those of PCL ($2\theta = 21.1$ and 23.3°). In PCL60LL40, the peaks at $2\theta = 16.5$ and 21.1° were also visible but had lower intensities than those of PCL80LL20. The PCL80EB20 displayed two small diffraction peaks associated with PCL (21.1 and 23.3°). The percent crystallinity obtained by XRD curves is shown in Table 6. PCL80LL20 demonstrated the highest percentage of PCL-associated crystallinity (~11%) among all samples. When the PLLA content increased to 40%, the percent crystallinity of PLLA also increased, though remained relatively small (2.64%).

The SAXS profiles of dried PU NPs are shown in Figure 8A. The characteristic peaks in PCL100 and PCL80LL20 revealed a *d*-spacing of 40 and 20 nm, respectively. In PCL60LL40 and PCL80EB20, the peak was not as distinct, though each curve had a peak corresponding to a *d*-spacing approximately at 11 and 9 nm.

3.3.3. FT-IR Spectra of PU. The FT-IR spectra of PU are demonstrated in Figure 8. The peak at ~3350 cm^{-1} was assigned to the hydrogen bonding of secondary amine groups in the hard segment. The absorption peaks near 1670 and 1730 cm^{-1} were each associated with the stretching of hydrogen-boned or free carbonyl group (C═O) in the urethane bond. The relative absorption at 1730 cm^{-1} (vs 1670 cm^{-1}) was much lower for PCL80LL20 in comparison to PCL100. This suggested that PCL80LL20 may have a higher portion of C═O group involved in hydrogen bonding than the other PUs. The FT-IR spectra for different PUs enlarged in the C═O stretching region are shown in Figure 8B. The fraction of hydrogen bonded C═O based on semiquantification of the individual peak areas after curve fitting is also listed. After

dx.doi.org/10.1021/am500213t | ACS Appl. Mater. Interfaces 2014, 6, 5685−5694

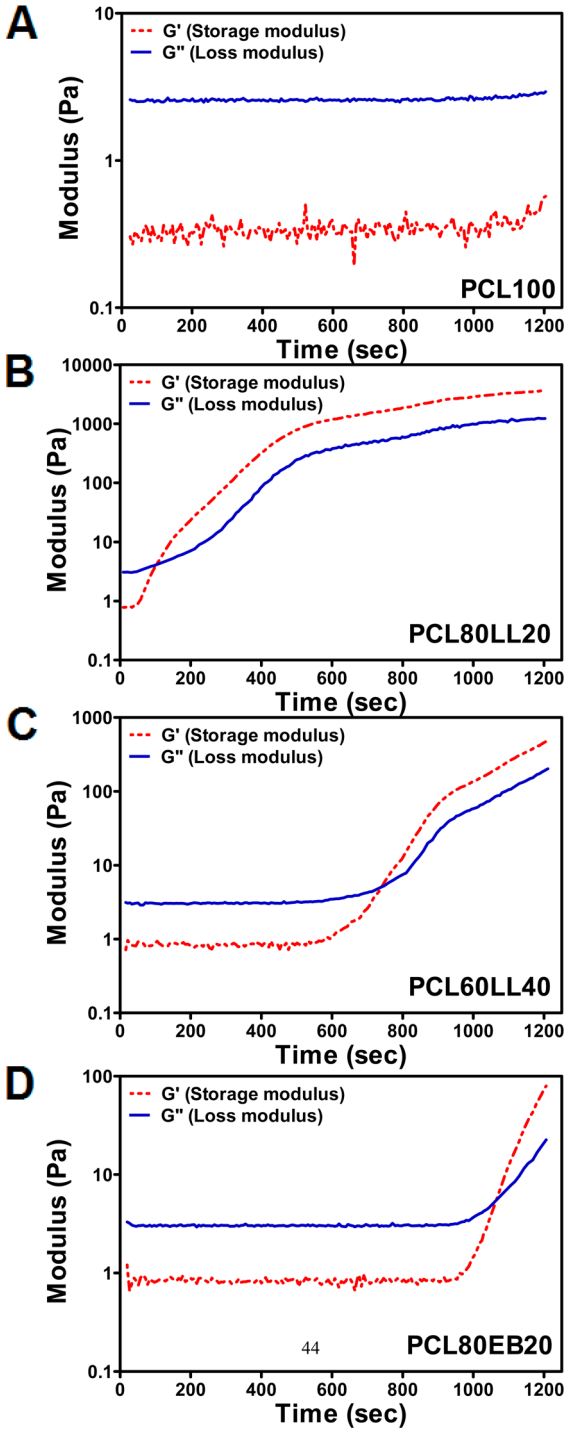

Figure 6. Storage modulus (G') and loss modulus (G'') of (A) PCL100, (B) PCL80LL20, (C) PCL60LL40, and (D) PCL80EB20 against treatment time at 37 °C.

Table 5. Rheological Properties of PU NP Dispersions Heated to 37°C

		cured gel (20 min)	
PU	gelation time (s)	G' (Pa)	G'' (Pa)
PCL100	NA	0.57	2.94
PCL80LL20	127	3618	1226
PCL60LL40	742	480	200
PCL80EB20	1103	76.17	21.32

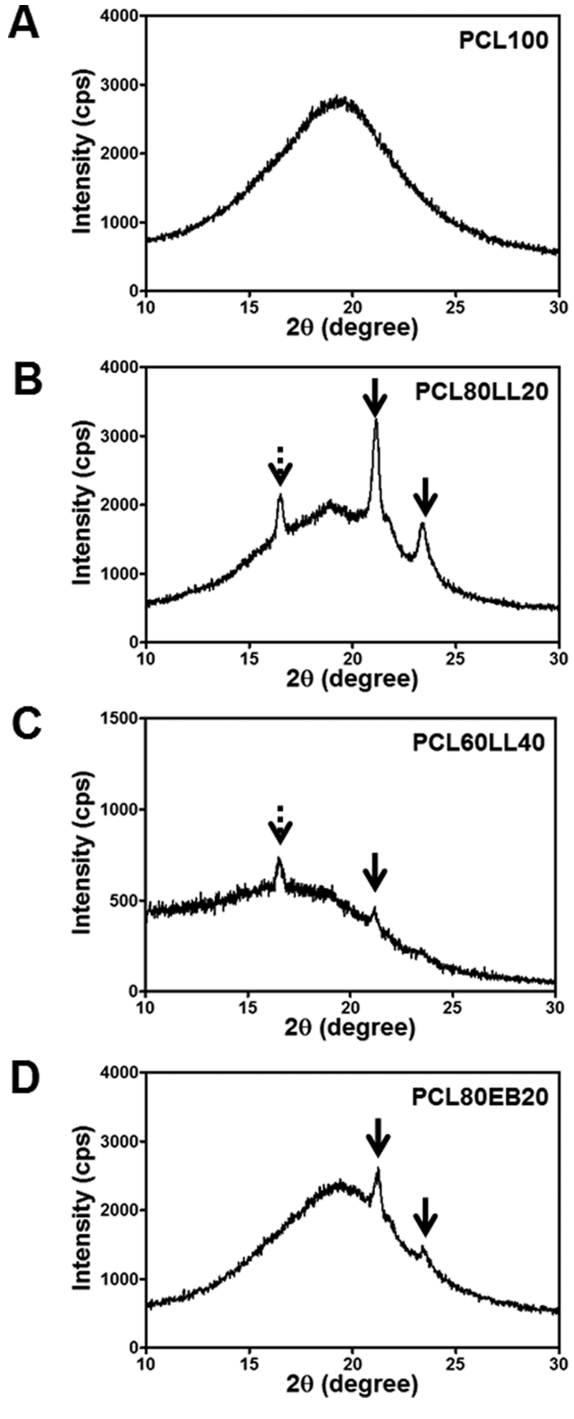

Figure 7. XRD profiles for dried (A) PCL100, (B) PCL80LL20, (C) PCL60LL40, and (D) PCL80EB20.

Table 6. Percentages of Crystallinity of PUs Obtained from XRD

PU	PLLA (2θ = 16.5°)	PCL (2θ = 21.1°)	PCL (2θ = 23.3°)
PCL100	NA	0	0
PCL80LL20	1.54	7.56	3.38
PCL60LL40	2.64	1.66	0.90
PCL80EB20	NA	2.18	0.65

semiquantification, PCL80LL20 revealed the largest fraction of the bonded C═O group followed by PCL60LL40.

dx.doi.org/10.1021/am500213t | ACS Appl. Mater. Interfaces 2014, 6, 5685−5694

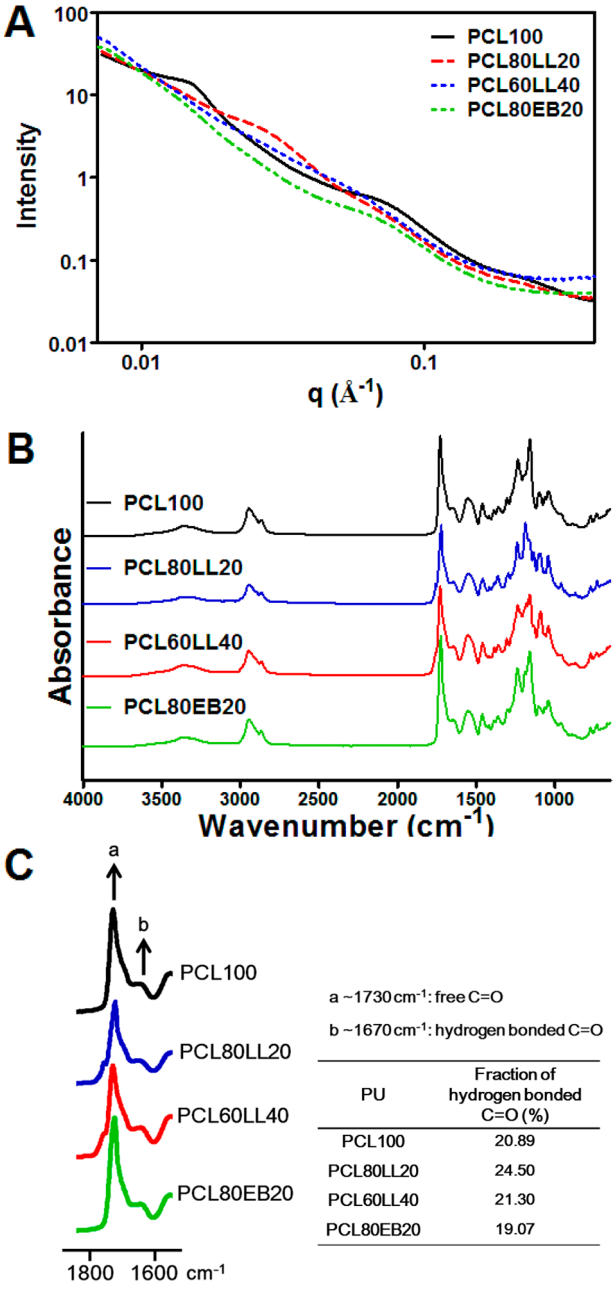

PU	Fraction of hydrogen bonded C=O (%)
PCL100	20.89
PCL80LL20	24.50
PCL60LL40	21.30
PCL80EB20	19.07

Figure 8. (A) SAXS profiles for dried PU NPs. (B) FT-IR spectra for different PUs and (C) FT-IR spectra for different PUs enlarged in C═O stretching region.

4. DISCUSSION

PU NP dispersions in four different soft segment compositions were successfully prepared by a green water-based procedure. The PU NPs were negatively charged because of the dissociation of −COOH group in hard segment. Judging from the zeta potential, the PU NPs were stably dispersed in water.[20] Although TEM examination revealed a relatively spherical morphology for the PU NPs, the shape factors obtained by AFFFF-MALS/DLS corresponded more to a worm-like structure.[21,22] We considered that the larger shape factors than expected may be ascribed to a shear-induced shape change when passing through the fractionation column. The deformation may result in an overestimation of R_g. In addition, AFFFF employed 0.1 M sodium nitrate as the eluent to avoid the channel blocking. The high ionic strength environment may produce a salting out effect that decreased the hydrodynamic size of PU NPs. The smaller values of R_h (Table 2) were apparent when compared to those obtained without fractionation (Table 3). The effect of salts on decreasing the NP size was different among NPs, i.e., the most evident for PCL80LL20 NPs and the least evident for PCL100. The overestimation of R_g and underestimation of R_h may be the reason behind the larger shape factors obtained by AFFFF-MALS/DLS analysis. On the other hand, this implies that our PU NPs may deform and pass through the capillaries when injected intravenously.

Regarding the compactness of the PU NPs, the N_{agg} values obtained from the study suggested a rather compact structure which might be due to the hydrophobic nature of PU chain. Moreover, the differences in chemical structure and flexibility between the two oligodiol segments (e.g., PLLA diol and PCL diol) may result in incompatibility of the interface and affect the aggregation state.[23] In our study, the less compact NP structure was observed in PCL80LL20 but not in PCL60LL40. This suggested that when the PLLA content reached 40 mol %, the PLLA segment may tend to gather and decrease the interface between the two oligodiol segments. At this time, the immiscibility between the two segments may no longer be obvious inside the NP. In the literature, the thermal properties of a polymer blend have been linked to the incompatibility between the two components.[24] The less compact structure of PCL80LL20 may enhance the mobility of chains inside the NP, resulting in a lower T_g. The better crystallinity of PLLA than PCL may contribute to a higher T_g of the PU with mixed compositions of soft segment. The PCL segment had a negative T_g and a softening temperature at about 50 °C while the PLLA segment had a T_g close to room temperature (25 °C). At temperatures higher than 25 °C, the PLLA chain may become mobile, which may account for the thermal sensitivity of the resulting polymer (PCL80LL20).

The size of NPs is an important parameter. The measurement of D_h is based on the Brownian motion and diffusion velocity which are mainly affected by the thermal properties. When the temperature increased from 10 to 37 °C, PCL100 NPs did not show much change in D_h, whereas PCL80LL20 revealed a significant increase in D_h. The incompatibility between PCL and PLLA and the greater microphase separation of PCL80LL20 may give rise to a large free volume and account for its significant thermally induced swelling. Once the NP was swollen, the mobility of water molecule might be limited by the hydrophobic PU backbone and result in an irreversible change in volume. When the content of PLLA increased to 40 mol % as in PCL60LL40, the repulsive force between soft and hard segments may be reduced. The more compact NP structure in PCL60LL40 further affected the thermal sensitivity. Conversely, the hydrophobic structure of PEBA diol and the similarity with PCL made PCL80EB20 NPs less swollen than PCL80LL20 NPs. The size enlargement at 25 °C was reversible for all PU NPs. When the temperature was raised above 25 °C, the polymer chains could undergo a wide range of adjustment and lead to an irreversible change in size. Moreover, the above-mentioned trend of R_h reduction in the presence of salt appeared to positively correlate with the thermoresponsiveness of the NPs, suggesting that the change of ionic interaction may be involved in regulating the thermal swelling properties of PU NPs.

The thermal dependence of morphology was further confirmed by TEM. Transformation from a spherical to rodlike

structure was observed for PCL80LL20 NPs upon heating to 37 °C. Such transformation may be caused by more secondary force (e.g., hydrogen bond) between soft segments at higher temperatures. However, the characteristic peak location in the SAXS profile did not shift with higher temperatures in any of the PU NP dispersions. This indicated that the distance between inner hard segment domains did not alter upon heating, though the size increases of NPs were observed for some PU formulas. As a partial of PCL was replaced by PLLA or PEB segments, the steric hindrance caused by the different soft segments could disturb the hard segment packing and increase the *d*-spacing (i.e., reduce the q value of the characteristic peak). This may make the R_g larger in PCL60LL40 and PCL80EB20. The shape factor obtained by SAXS (R_g) and DLS (R_h) was smaller than that based on AFFFF analysis, indicating a more spherical structure. Among all PU NPs, a greater shape factor for PCL80LL20 NPs was observed at 37 °C because of the thermally induced swelling. The $M_{w,\,NP}$ obtained from the Kratky method was in a magnitude of 1×10^4 kDa for each type of PU NPs, confirming the tight structure of the NPs. Because the Kratky method for molecular weight determination assumed a density close to 1 g/cm^3, the values were just estimations.

PU NPs in this study showed a range of swelling behavior. PCL100 NPs had very limited swelling under 37 °C probably because the distance between NPs was too long to have interactions.[25] For PCL80LL20, the distance between NPs was probably shortened at 37 °C and the sol−gel transition may occur rapidly as a result of more interaction. PCL60LL40 and PCL80EB20 NPs had smaller swelling ratios and volumetric changes and a longer time was required for them to reach equilibrium when compared to PCL80LL20 NPs. Aggregation of soft segment normally occurs along the microphase separation. In PCL100, the mobility of soft segment may be restricted by the hard segment and thus an ordered structure may not form easily. SAXS of dried PCL100 NPs showed a longer *d*-spacing, suggesting poor chain mobility. On the basis of XRD, PCL80LL20 had a higher percentage of ordered structure than PCL100. When PLLA was added to replace a fraction of PCL, the steric hindrance and the nonhomogeneous secondary force between soft segments may facilitate each of PCL and PLLA to arrange itself more efficiently. This may account for the emergence of crystalline peaks associated with both PLLA and PCL. Such an advantage was missing in PCL60LL40 where the interface between two soft segments decreased. Therefore, the intensity of crystalline peaks was reduced in PCL60LL40. PEBA may be more easily adapted to PCL structure, so the effect of crystallinity enhancement in PCL80EB20 was not as obvious as in PCL80LL20. Nevertheless, small crystalline peaks of PCL were still seen in the XRD of PCL80EB20.[26] Overall, mixing a second soft segment enhanced the crystallinity of PCL-based PU, which was an unexpected finding of the study.

FT-IR spectroscopy further confirmed the changes in hydrogen bonding among different PUs. A typical hydrogen bond in PU involves the amide group as the donor and the carbonyl group as the acceptor, mainly in hard segments.[27,28] FT-IR spectra revealed a higher fraction of hydrogen-bonded carbonyl group in PCL80LL20 and PCL60LL40, indicating a greater degree of microphase separation.[29] The secondary force may further affect the behavior of chain-folding and swelling.[30] The amorphous nature of PCL100 could restrict its ability to self-assemble. In fact, we observed that the thermal swelling of PCL100 occurred only when the temperature was raised to 50−55 °C. In contrast, swelling and gelation occurred in PCL80LL20 near body temperature.

Based on the physicochemical characterization and the above arguments, a hypothetical mechanism for the thermally induced gelation of PU NPs (ranking in the order of PCL80LL20 > PCL60LL40 > PCL80EB20 > PCL100) is depicted in Figure 9.

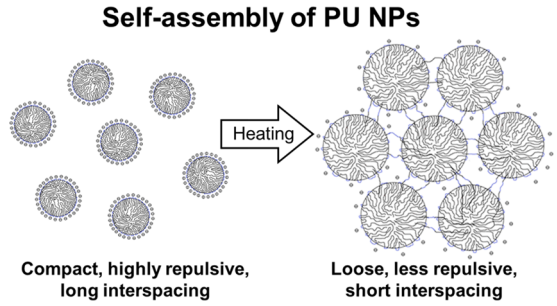

Figure 9. Possible mechanisms for the temperature-induced self-assembly and swelling.

The chain mobility of PU NPs is enhanced by raising the temperature, whereas a partial of −COOH group no longer orients outward. The shorter distance arising from size expansion/swelling and lower repulsive force among PU NPs may result in aggregation and further lead to a macroscopic sol−gel transition. An in-depth study is necessary for elucidation of the structural formation mechanism. For example, more SAXS and rheological analyses at different temperatures near phase transition may help clarify the detailed mechanisms behind the phenomena.

Finally, the effects of mixing two oligodiols with different crystallinity and flexibility on the microstructure change and thermal sensitivity of PU NPs were beyond anticipation. The sol−gel transition of PCL80LL20 at 37 °C could be applied in cell encapsulation (see the Supporting Information, Figures S2 and S3) or other potential biomedical applications. In particular, the PU synthesized in this study is biodegradable. It was expected that a series of bioabsorbable thermo-responsive smart polymers based on a combination of different biodegradable soft segment compositions may be developed in the future.

5. CONCLUSIONS

In this study, we employed a combination of ester-type oligodiols to prepare PU NP dispersions from a water-based procedure. The PU NPs prepared were compact spheres which were swollen in various degrees when the temperature was raised to 37 °C. The relatively loose structure of PCL80LL20 NPs but not the other NPs was caused by the immiscibility between PCL diol and PLLA diol. The large shape factors (1.27−1.66) in the shear state suggested the deformability of the NPs. The thermal responsiveness of PCL80LL20 NPs may be attributed to the ordered structure at lower temperatures that became mobile at higher temperatures. A larger swelling ratio (∼450%) and faster gelation time (∼130 s) were observed for the dispersion of PCL80LL20 when the temperature approached 37 °C. The analyses of XRD and FT-IR confirmed the more extensive microphase separation and larger extent of crystallinity for PCL80LL20 NPs. The significant self-assembly behavior of PCL80LL20 NPs near body temperature may be

potentially useful for designing smart carriers for delivery of cells or drugs.

■ ASSOCIATED CONTENT

Supporting Information

The thermal dependence of zeta potential for PU NPs (Figure S1), the survival of stem cells encapsulated in gel of PCL80LL20 NPs (Figure S2), and the ^{1}H NMR spectrum of PCL100 NPs (Figure S3). This material is available free of charge via the Internet at http://pubs.acs.org/.

■ AUTHOR INFORMATION

Corresponding Author

*E-mail: shhsu@ntu.edu.tw. Phone: (886) 2-33665313. Fax: (886) 2-33665237.

Notes

The authors declare no competing financial interest.

■ ACKNOWLEDGMENTS

This research was supported by the National Research Program for Nanoscience and Technology of the National Science Council (NSC 101-2120-M-002-002), Taiwan. We are also obliged to the Precious Instrument Center of National Taiwan University and Ms. C.-Y. Chien for providing the TEM facility and technical assistance.

■ REFERENCES

(1) Zohuriaan-Mehr, J. M.; Kabiri, K. Superabsorbent Polymer Materials: A Review. *Iran. Polym. J.* **2008**, *17*, 451−477.
(2) Hoffman, A. S. Hydrogels for Biomedical Applications. *Adv. Drug Delivery Rev.* **2002**, *54*, 3−12.
(3) Schmaljohann, D. Thermo- and pH-Responsive Polymers in Drug Delivery. *Adv. Drug Delivery Rev.* **2006**, *58*, 1655−1670.
(4) Gupta, P.; Vermani, K.; Garg, S. Hydrogels: from Controlled Release to pH-Responsive Drug Delivery. *Drug Discovery Today* **2002**, *7*, 569−579.
(5) Liu, F.; Urban, M. W. Recent Advances and Challenges in Designing Stimuli-Responsive Polymers. *Prog. Polym. Sci.* **2010**, *35*, 3−23.
(6) Hoare, T. R.; Kohane, D. S. Hydrogels in Drug Delivery: Progress and Challenges. *Polymer* **2008**, *49*, 1993−2007.
(7) Tong, F.; Chen, X.; Chen, L.; Zhu, P.; Luan, J.; Mao, C. Preparation, Blood Compatibility and Anticoagulant Effect of Heparin-Loaded Polyurethane Microspheres. *J. Mater. Chem. B* **2013**, *1*, 447−453.
(8) Bil, M.; Ryszkowska, J.; Woźniak, P.; Kurzydłowski, K. J.; Lewandowska-Szumieł, M. Optimization of The Structure of Polyurethanes for Bone Tissue Engineering Applications. *Acta Biomater.* **2010**, *6*, 2501−2510.
(9) Jovanovic, D.; Engels, G. E.; Plantinga, J. A.; Bruinsma, M.; van Oeveren, W.; Schouten, A. J.; van Luyn, M. J. A.; Harmsen, M. C. Novel Polyurethanes with Interconnected Porous Structure Induce In Vivo Tissue Remodeling and Accompanied Vascularization. *J. Biomed. Mater. Res.* **2010**, *95A*, 198−208.
(10) Oertel, G. *Polyurethane Handbook*; Hanser Publishers: Munich, 1994.
(11) Yang, J. E.; Lee, Y. H.; Koo, Y. S.; Jung, Y. J.; Kim, H. D. Preparation and Properties of Waterborne Poly(urethane-urea) Ionomers Effect of The Type of Neutralizing Agent. *Fibers Polym.* **2002**, *3*, 97−102.
(12) Kohjiya, S.; Ikeday, Y.; Takesako, S.; Yamashita, S. Drug Release Behavior from Polyurethane Gel. *React. Polym.* **1991**, *15*, 165−175.
(13) Tanaka, Y.; Gong, J. P.; Osada, Y. Novel Hydrogels with Excellent Mechanical Performance. *Prog. Polym. Sci.* **2005**, *30*, 1−9.
(14) Park, D.; Wu, W.; Wang, Y. A Functionalizable Reverse Thermal Gel Based on A Polyurethane/PEG Block Copolymer. *Biomaterials* **2011**, *32*, 777−786.
(15) Chao, G. T.; Qian, Z. Y.; Huang, M. J.; Kan, B.; Gu, Y. C.; Gong, C. Y.; Yang, J. L.; Wang, K.; Dai, M.; Li, X. Y.; Gou, M. L.; Tu, M. J.; Wei, Y. Q. J. Synthesis, Characterization, and Hydrolytic Degradation Behavior of A Novel Biodegradable pH-Sensitive Hydrogel Based on Polycaprolactone, Methacrylic Acid, and Poly(ethylene glycol). *J. Biomed. Mater. Res.* **2008**, *85A*, 36−46.
(16) Zhao, S. P.; Cao, M. J.; Li, L. Y.; Xu, W. L. Synthesis and Properties of Biodegradable Thermo- and pH-Sensitive Poly[(N-isopropylacrylamide)-co-(methacrylic acid)] Hydrogels. *Polym. Degrad. Stab.* **2010**, *95*, 719−724.
(17) Zheng, Y.; He, C.; Huynh, C. T.; Lee, D. S. Biodegradable pH- and Temperature-Sensitive Multiblock Copolymer Hydrogels Based on Poly(amino-ester urethane)s. *Macromol. Res.* **2010**, *18*, 974−980.
(18) Jeonga, B.; Baeb, Y. H.; Kima, S. W. Drug Release from Biodegradable Injectable Thermosensitive Hydrogel of PEG−PLGA−PEG Triblock Copolymers. *J. Controlled Release* **2000**, *63*, 155−163.
(19) Taiwan patents (I427091 approval and 102100076 pending) and U.S. patent applications (13/317,651 Biodegradable and biocompatible waterborne polyurethane and 14/145,393 Biocompatible and biodegradable elastomer).
(20) Noble, K. L. Waterborne Polyurethanes. *Prog. Org. Coat.* **1997**, *32*, 131−136.
(21) Zhua, Z.; Xiea, C.; Liub, Q.; Zhena, X.; Zhenga, X.; Wua, W.; Lib, R.; Dingc, Y.; Jianga, X. The Effect of Hydrophilic Chain Length and iRGD on Drug Delivery from Poly(ε-caprolactone)-Poly(N-vinylpyrrolidone) Nanoparticles. *Biomaterials* **2011**, *32*, 9525−9535.
(22) Tande, B. M.; Wagner, N. J.; Mackay, M. E.; Hawker, C. J.; Jeong, M. Viscosimetric, Hydrodynamic, and Conformational Properties of Dendrimers and Dendrons. *Macromolecules* **2001**, *34*, 8580−8585.
(23) Cohn, D.; Salomon, A. H. Designing Biodegradable Multiblock PCL/PLA Thermoplastic Elastomers. *Biomaterials* **2005**, *26*, 2297−2305.
(24) Sakai, F.; Nishikawa, K.; Inoue, Y.; Yazawa, K. Nucleation Enhancement Effect in Poly(L-lactide) (PLLA)/Poly(ε-caprolactone) (PCL) Blend Induced by Locally Activated Chain Mobility Resulting from Limited Miscibility. *Macromolecules* **2009**, *42*, 8335−8342.
(25) Hamner, K. L.; Maye, M. M. Thermal Aggregation Properties of Nanoparticles Modified with Temperature Sensitive Copolymers. *Langmuir* **2013**, *29*, 15217−15223.
(26) Bai, H.; Xiu, H.; Gao, J.; Deng, H.; Zhang, Q.; Yang, M.; Qiang Fu, Q. Tailoring Impact Toughness of Poly(L-lactide)/Poly(ε-caprolactone) (PLLA/PCL) Blends by Controlling Crystallization of PLLA Matrix. *ACS Appl. Mater. Interfaces* **2012**, *4*, 897−905.
(27) Tan, H.; Li, J.; Guo, M.; Du, R.; Xie, X.; Zhong, Y.; Fu, Q. Phase Behavior and Hydrogen Bonding in Biomembrane Mimicing Polyurethanes with Long Side Chain Fluorinated Alkyl Phosphatidylcholine Polar Head Groups Attached to Hard Block. *Polymer* **2005**, *46*, 7230−7239.
(28) Coleman, M. M.; Skrovanek, D. J.; Hu, J.; Painter, P. C. Hydrogen Bonding in Polymer Blends. 1. FTIR Studies of Urethane-Ether Blends. *Macromolecules* **1988**, *21*, 59−65.
(29) Jiang, X.; Li, J.; Ding, M.; Tan, H.; Ling, Q.; Zhong, Y.; Fu, Q. Synthesis and Degradation of Nontoxic Biodegradable Waterborne Polyurethanes Elastomer with Poly(ε-caprolactone) and Poly(ethylene glycol) as Soft Segment. *Eur. Polym. J.* **2007**, *43*, 1838−1846.
(30) Mondal, T.; Dan, K.; Deb, J.; Jana, S. S.; Ghosh, S. Hydrogen-Bonding-Induced Chain Folding and Vesicular Assembly of an Amphiphilic Polyurethane. *Langmuir* **2013**, *29*, 6746−6753.